The Journal of Experimental Biology 211, 3442-3453
Published by The Company of Biologists 2008
doi:10.1242/jeb.022608

Non-linear intramolecular interactions and voltage sensitivity of a K_V1 family potassium channel from *Polyorchis penicillatus* (Eschscholtz 1829)

Tara L. Klassen[1], Megan L. O'Mara[2], Megan Redstone[2], Andrew N. Spencer[1,3] and Warren J. Gallin[1,*]

[1]Department of Biological Sciences, University of Alberta, Edmonton, Alberta, Canada T6G 2E9, [2]Department of Biological Sciences, University of Calgary, Calgary, Alberta, Canada T2N 1N4 and [3]Malaspina University College, 900 Fifth Street, Nanaimo, British Columbia, Canada V9R 5S5

*Author for correspondence (e-mail: wgallin@ualberta.ca)

Accepted 2 September 2008

SUMMARY

Voltage sensitivity of voltage-gated potassium channels (VKCs) is a primary factor in shaping action potentials in excitable cells. Variation in the amino acid sequence of the channel proteins is responsible for differences in the voltage range over which the channel opens. Thus, understanding how changes in voltage sensitivity are effected by changes in channel protein sequence illuminates the functional evolution of excitability. The K_V1-family channel jShak1, from the jellyfish *Polyorchis penicillatus*, differs from most other K_V1 channels in ways that are useful for studying the problem of how voltage sensitivity is related to channel sequence. We assessed the contributions of changes in sequence of the S4, voltage sensing, helix and changes in one asparagine residue in the S2 helix, to the relative stability of the open and closed states of the channel. Mutation of the neutral S2 residue (Asn227) to glutamate stabilized the open conformation of the channel. Different modifications of charge and length in S4 favoured either the closed conformation or the open conformation. The interactions between pairs of mutations revealed that some of the S4 mutations alter the conformation of the voltage-sensing domain such that the S4 helix is constrained to be closer to the S2 helix than in the wild-type conformation. These results, taken in conjunction with three-dimensional models of the channel, identify intra-molecular interactions that control the balance between open and closed states. These interactions are likely to be relevant to understanding the functional characteristics of members of this channel family from other organisms.

Supplementary material available online at http://jeb.biologists.org/cgi/content/full/211/21/3442/DC1

Key words: site-directed mutagenesis, ion channel gating, electrophysiology.

INTRODUCTION

Voltage-gated potassium channels of the Shaker superfamily open in response to depolarization of the membrane. Members of the K_V1 (Shak) subfamily express currents with fast opening kinetics, followed by either or both a rapid (N-type) or slower (C-type) inactivation. The voltage sensitivities of activation and inactivation are critical to the role that these channels play in shaping action potentials and modifying the firing properties of neurons and other excitable cells (Connor and Stevens, 1971a; Connor and Stevens, 1971b; Connor and Stevens, 1971c; Guan et al., 2007; Kasten et al., 2007). Understanding how the amino acid sequence of channel proteins affects their voltage sensitivity is important for understanding how genetic variation can cause changes in action potential form and excitability patterns, and ultimately how different excitability properties have evolved.

The S4 transmembrane helical segment of voltage-gated ion channels is the voltage sensor (Guy et al., 1991; Noda et al., 1984). This segment contains a basic amino acid at every third position along the length of the helix in the form Arg-Xaa-Xaa or Lys-Xaa-Xaa. Since this charged helix traverses the plasma membrane, changes in membrane potential exert a force on the helix, causing it to move and change the conformation of the channel. Each charged motif does not contribute equally to voltage sensing (Bezanilla et al., 1994; Papazian et al., 1995; Seoh et al., 1996). Furthermore, the potential field of the membrane is not distributed completely or evenly over the S4 segment but is focused by aqueous 'canals' on both sides of the channel protein near the S4 transmembrane helix (Ahern and Horn, 2005; Baker et al., 1998; Chanda et al., 2005; Islas and Sigworth, 2001; Starace and Bezanilla, 2004; Yang and Horn, 1995).

Residues external to the S4 transmembrane helix also contribute to voltage sensitivity of channel activation (Monks et al., 1999; Papazian et al., 1995; Perozo et al., 1999; Tiwari-Woodruff et al., 2000). In the *Drosophila melanogaster* Shaker channel, the closed conformation is stabilized by salt bridges formed between Lys374 (K374) in S4 and Glu293 (E293) and Asp316 (D316) in S2 and S3, respectively (Durell et al., 2004; Li-Smerin et al., 2000; Papazian et al., 1995; Tiwari-Woodruff et al., 1997). The open conformation is stabilized by the interaction of Arg368 (R368) and R371 in S4 with E283 in the S2 transmembrane helix, whereas E293 in S2 and D316 in S3 interact with R377 (Papazian et al., 1995; Silverman et al., 2003). A neutralization mutant of E293 destabilizes the closed conformation, shifting the voltage sensitivity of *Drosophila* Shaker in a hyperpolarized (leftward) direction whereas neutralization mutants of E283 and D316 shift the voltage sensitivity of these channels in a depolarizing (rightward) direction (Papazian et al., 1995).

The physical factors that affect the voltage of half activation (V_{50}) of a channel can be partitioned into two parameters, the gating charge that moves in response to a change in membrane potential, and the relative difference of internal free energy of the protein in the open and closed states. At a membrane potential of 0 mV, the channel partitions into open and closed states as a function of the internal energy difference between the two states. When a membrane

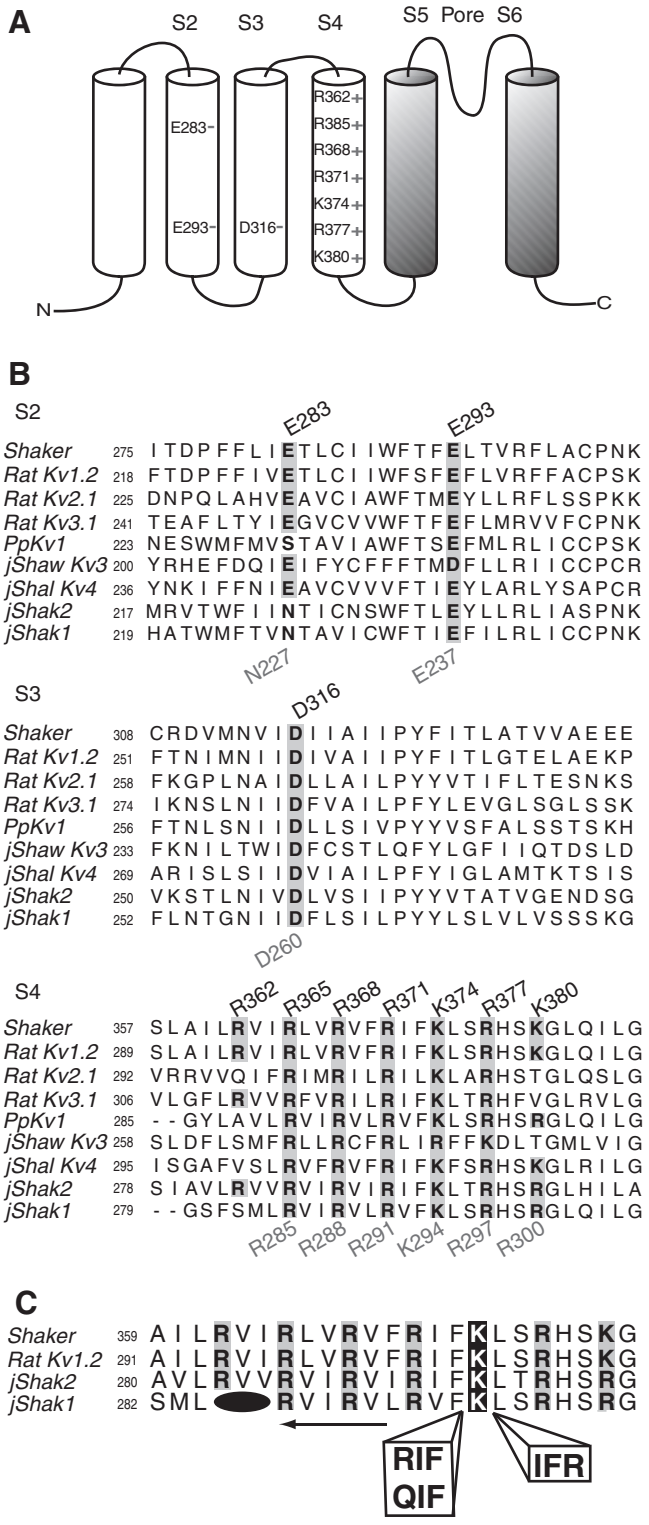

Fig. 1. The jShak1 channel lacks one acidic residue in S2 and one basic triplet motif in S4, compared with *Drosophila* Shaker and RatK_V1.2. (A) A schematic of a single 6TM alpha subunit of the *Drosophila* Shaker voltage-gated potassium channel. The S5-pore, S5-S6 loop and S6 domain are shown in grey and the S1-S4 transmembrane helices are white. The conserved acidic residues in S2 and S3 are labelled as are the characteristic basic residues in S4. (B) Alignments of the transmembrane helices S2, S3 and S4 in selected *Drosophila*, rat and hydrozoan K_V channels. The jellyfish (*Polyorchis penicillatus*) channel jShak1 lacks one (N227) of the two acidic residues in S2 but contains the stabilizing acidic residue (D260) in S3. The S4 voltage sensor of jShak1 lacks one basic motif found in other K_V1 channels but has the same helical length. The highly conserved acidic residues (E283 and E293) in S2 and the conserved acidic residue (D316) in S3 and the basic residues in the S4 voltage sensor of *Drosophila* Shaker and other Shaker-type channels are highlighted in grey. (C) Alignment of the S4 helix of jShak1 with the S4 helices of three other channels, indicating the sites of insertion of the S4 mutants used in this study on either side of position K294 (highlighted in black) in jShak1.

potential is applied, an additional energy term is added, the energy difference between the gating charge in the open-state *versus* the closed state conformation, proportional to the product of the gating charge and the voltage of the potential field. This additional energy term shifts the equilibrium between the open and closed states. Conversely, by experimentally determining the V_{50} and the gating charge of the channel, it is possible to calculate the Gibb's free energy (ΔG_0) for channel opening. By evaluating the differences in ΔG_0 of various mutations it is then possible to define the way in which intra-molecular interactions determine ΔG_0, gating charge, and thus the voltage sensitivity. Using the formalism in this study, the probability that the channel is closed increases as the ΔG_0 increases.

Fig. 1A illustrates the general transmembrane topology of the K_V family potassium channel proteins, annotated with the positions of the residues discussed in this paper form the *D. melanogaster* Shaker channel. The K_V1 channels (jShak1 and jShak2) from the jellyfish, *Polyorchis penicillatus*, differ from all other, non-cnidarian, K_V channels in that a residue in S2 that is usually a conserved acidic residue (E283 in *Drosophila* Shaker channels), is a neutral asparagine (N227), and the loop that links the S3 and S4 helices is very short, constraining their relative motion. The V_{50} values of both *Polyorchis* channels are markedly more positive than those of homologous vertebrate K_V1 channels (Grigoriev et al., 1997; Jegla et al., 1995). In comparison with most other K_V1 channels (including jShak2), jShak1 has one less positively charged motif in the S4 region, with a charged residue being absent at the position equivalent to R362 in *Drosophila* Shaker (Fig. 1). The recently cloned K_V1 channel from the Portuguese Man-o-War, *Physalia physalis*, also lacks the first acidic residue in S2 (S231 in PpK_v1) and has a shortened S4 (Bouchard et al., 2006), suggesting that these two structural differences may reflect a conserved variant of K_V1 channel architecture in the class Hydrozoa. Previous mutagenesis analysis in *jShak1* (Grigoriev et al., 1997) demonstrated that the addition of length and charge in the S4 voltage sensor, to either side of the conserved K294 residue (K374 in *Drosophila* Shaker) had complex effects on channel properties, but did not simply shift the voltage sensitivity of jShak1 to the range observed for vertebrate K_V1 channels.

The current study was designed to determine how interactions between N227 and the S4 helix of jShak1 affect voltage sensitivity by setting the gating charge and the internal energy difference between open and closed states.

MATERIALS AND METHODS

Construction of expression plasmids

The wild-type *jShak1* coding region contained in the BlueScript plasmid (Grigoriev et al., 1997; Jegla et al., 1995) was amplified using primers WJG1182 and WJG1173 (Table S1 in supplementary material). The PCR fragment was cut using unique

*Xho*I and *Spe*I sites and was inserted into the pXT7 plasmid and sequenced to confirm that no PCR-induced errors were present. Translational efficiency of transcribed mRNA is enhanced by using pXT7 as the expression vector because the inserted coding region is flanked by 5′ UTR and 3′ UTR sequences from *Xenopus laevis* globin mRNA.

To produce a non-inactivating channel, the full-length *jShak1* in pXT7 was used as a template for PCR amplification with primers WJG 2037 and WJG 1246 (Table S1 in supplementary material). The PCR fragment and the wild-type expression plasmid were cut with *Xho*I and *Hpa*I (New England Bioloabs, Ipswich, MA, USA) at unique restriction sites. The PCR product was then ligated into the wild-type plasmid, to create a Δ23 N-truncated channel without the N-type inactivation ball, as described previously (Jegla et al., 1995). By removing fast, N-type inactivation (Hoshi et al., 1990) the steady-state conductance of the channels can be more accurately measured from tail currents. This channel was designated as 'wild type' for all subsequent experiments.

The triplet mutations of the S4 sensor, whereby either Arg-Ile-Phe (RIF) or Gln-Ile-Phe (QIF) was inserted on the N-terminal side of K294, or Ile-Phe-Arg (IFR) was inserted on the C-terminal side of K294 (Fig. 1C), were constructed in this plasmid as described previously (Grigoriev et al., 1997). The S2 mutations at Asn227 (N227; Fig. 1B) were created by overlapping PCR mutagenesis. Primers used to create the N227E mutation were WJG1062 and WJG1063 and construction of N227D used primers WJG1064 and WJG1065. In both instances the flanking primers were WJG1149 and WJG1181. The resulting PCR products were digested with *Hpa*I and *Cla*I and ligated into the wild-type or S4 mutant plasmids to create single (S2) and double (S2/S4) mutations, respectively. The sequence of all mutants was confirmed to be as designed by sequencing the cloned plasmid with the two flanking primers WJG1149 and WJG1181.

Expression plasmids and oocyte preparation

Purified plasmids were prepared from 10 ml overnight cultures [Terrific Broth (Ausubel et al., 1987) with 100 μg ml^{-1} ampicillin] using a Wizard Miniprep Kit (Promega, Madison, Wisconsin, USA). Plasmids were linearized with *Xba*I and gel purified using the QiaQuick Gel Extraction Kit (Qiagen, Mississauga, ON, Canada). Capped mRNAs were prepared by *in vitro* transcription using a mMessage mMachine (Ambion, Austin, TX, USA) T7 polymerase kit, and stored at –80°C.

Female *X. laevis* that were 2 years old were reversibly anaesthetized in 0.17% MS-222 (Sigma, St Louis, MO, USA) and a single lateral incision made in the abdomen 1 cm from the midline, 1 cm caudal to the pelvic girdle. A single ovary was removed and manually separated into 0.5 cm clumps. Ovarian pieces were rinsed three times in MBM [in mmol l^{-1}: NaCl 88, KCl 1, $Ca(NO_3)_2$ 0.33, $CaCl_2$ 0.41, $MgSO_4$ 0.82, $NaHCO_3$ 2.4, Hepes 10 (Tris base to pH 7.5), sodium pyruvate 2.5, supplemented with penicillin G 0.1 g l^{-1} and gentamycin sulphate 0.05 g l^{-1} (Huang et al., 1993)]. The tissue fragments were incubated on a rotating shaker in 2 mg ml^{-1} collagenase 1A (Sigma, Oakville, ON, Canada) in MBM at room temperature. Released oocytes were removed from the collagenase solution after 2 h, rinsed in MBM and ~200 eggs incubated per glass scintillation vial, at 17°C overnight in fresh MBM. Eggs were de-folliculated by immersion in a hypo-osmotic phosphate buffer [in mmol l^{-1}: K_2PO_4 100 (pH 6.5 with HCl)] for 1 h. Following treatment, eggs were left for 2 h in fresh MBM to recover prior to manipulation. Mature stage V–VII oocytes were injected with 48.6 nl mRNA (200–600 ng nl^{-1}) and incubated in MBM at 17°C.

Electrophysiological methods

The N-truncated jShak1 wild-type channel had identical activation properties to the full-length channel, but lacked fast N-type inactivation (Jegla et al., 1995) (Fig. 2A,B). The channels expressed in pXT7 had higher rates of translation compared to mRNA prepared from BlueScript (Grigoriev et al., 1997; Jegla et al., 1995), but had identical electrophysiological properties. The mutants manifested variable C-type inactivation, with IFR-E having the most inactivation at 150 ms, but all channels opened quickly, allowing for peak currents to be obtained within 50 ms. Therefore, all electrophysiological protocols were designed to provide current measurements prior to significant C-type inactivation (Fig. 2C,D).

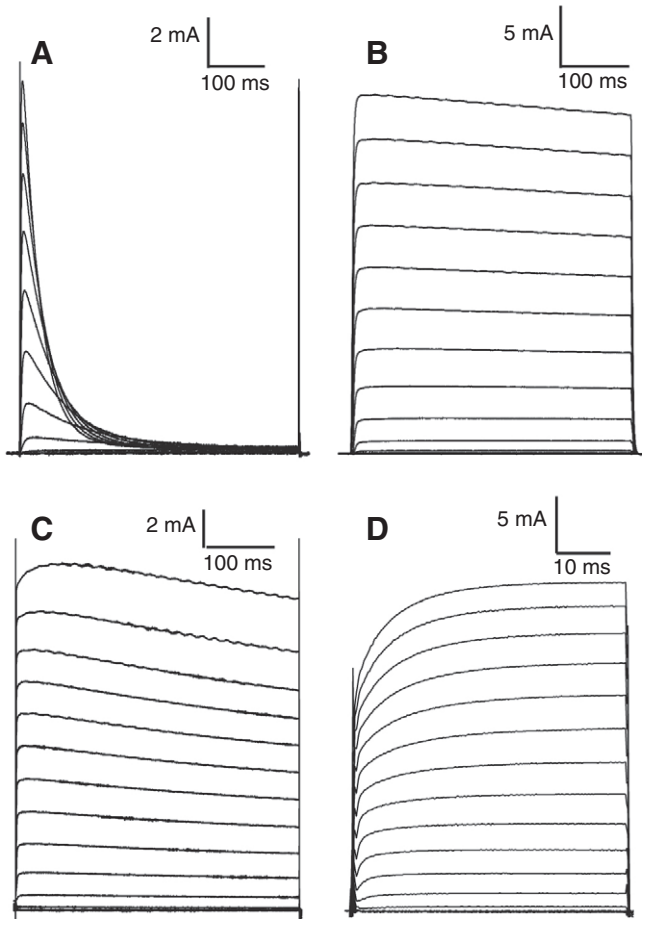

Fig. 2. Δ23 N-truncated jShak1 channels lack N-type inactivation but exhibit slow C-type inactivation. (A) The full-length wild-type jShak1 channel expressed fast opening kinetics and fast N-type inactivation in *Xenopus* oocytes. Outwardly directed current traces were evoked by 500 ms step depolarizations from a holding potential of –90 mV to a range of potentials from –90 to +90 mV in 10 mV increments followed by a return to –90 mV. (B) The Δ23 N-truncated wild-type *jShak1* channel lacked N-type inactivation. Outwardly directed current traces were evoked by 400 ms step depolarizations from a holding potential of –90 mV to a range of potentials from –90 to +90 mV in 10 mV increments followed by a return to the holding potential. (C) The IFR-E double mutant expressed slow, C-type inactivation. Other N-truncated S2/S4 mutant jShak1 channels showed lesser amounts of slow inactivation. Currents evoked as in B. (D) Shortened acquisition protocols allowed channels to open fully but limited the amount of slow inactivation. Outwardly directed currents from an IFR-E mutant evoked by 50 ms step depolarizations from a holding potential of –90 mV to a range of potentials from –90 to +90 mV in 10 mV increments followed by a 20 ms step to –50 mV and 200 ms return to holding potential.

Electrophysiological measurements on all channels were performed 2 days after injection. Oocytes were impaled with glass microelectrodes fabricated from borosilicate glass, filled with 3 mol l^{-1} KCl and having resistances between 0.5 and 1 MΩ. Voltage-clamp recordings were obtained using a GeneClamp 500B amplifier (Axon Div., Molecular Devices, Sunnyvale, CA, USA) controlled by pClamp 9.0 software (Axon Div., Molecular Devices). Data were acquired through a 1322A analogue/digital converter and analysed using Clampfit 9.0 (Axon Div., Molecular Devices). Experiments were performed in ND96 (in mmol l^{-1}: NaCl 96, KCl 2, $CaCl_2$ 1.8, $MgCl_2$ 1, Hepes 5, pH 7.4). Measurements were performed with leak subtraction (P/N=4) for all constructs.

Steady-state conductance was measured using a pulse protocol where the membrane is held at –90 mV for 10 ms, followed an activation test pulse from –140 mV to +90 mV in 2 mV steps for a duration of 50 ms. This was followed by a 20 ms tail-step to –120 mV for inward tails or –50, or –30 mV for outward tails, followed by a 200 ms return to a –90 mV holding potential (see Fig. S1 in supplementary material for examples of traces from a simplified –30 mV tail-step protocol). Because the deactivation kinetics in jShak1 are voltage dependent, with channels closing rapidly at hyperpolarized voltages, it was not always possible to use inward tail currents for steady-state conductance measurements, and outward tail currents were utilized. It is important to note that the S4 single and double mutations shifted the threshold for channel activation such that some channels (see Fig. S1 in supplementary material; N227E) were open at the –30 mV tail-step, and the –50 mV tail-step protocol was used for subsequent data analysis. Steady-state voltage-conductance curves were obtained by fitting the tail current to the sum of two exponential decays to increase detection of low probability opening events near the threshold voltage. The resultant fitted parameters were used to obtain calculated current values at 2 ms following the capacitative transient artefact (see Fig. S2 in supplementary material). These current values were normalized using a four-parameter Boltzmann curve (see below) to obtain a normalized measure of conductance.

The calculated current *vs* voltage data were fitted with a four-parameter Boltzmann curve:

$$I = y_0 + \left[\frac{I_{max}}{\left(1 + e\left(\frac{-\left(V - V_{50}\right)}{b} \right) \right)} \right], \quad (1)$$

where y_0 is an offset, I_{max} is maximal current, V is the voltage of the depolarizing pulse, V_{50} is the voltage at which half of the channels are activated, and b is the Boltzmann slope factor. Since the tail currents were measured at a constant voltage, the conductance, G, at a given depolarization potential is proportional to the tail current, I, and the results have been represented graphically as G/G_{max} *vs* depolarizing voltage.

Although it is possible to calculate a charge associated with the transition between two states from the Boltzmann slope factor (b), this derivation is only valid for a two-state equilibrium. The transition between the open and the closed state of VKCs involves a large number of intermediate states, each with their own voltage dependency (Almers, 1978; Sigg and Bezanilla, 1997). The result of this complexity is that the charge calculated from the Boltzmann slope factor consistently underestimates the gating charge, and that the difference between the estimate and the true gating charge varies as a complicated function of the intermediate states. Almers derived a robust method for estimating gating charge, by determining the limiting slope of the $\log(G/G_{max})$ *vs* V curve at very low conductance (Almers, 1978). This estimate of gating charge approaches the true gating charge asymptotically. Sigg and Bezanilla demonstrated that the absolute value of the gating charge determined by the limiting slope method is insensitive to the nature of the state transitions in a number of realistic scenarios (Sigg and Bezanilla, 1997). An example of this analysis, including determination of the asymptotic value, as implemented by Gonzalez et al. (Gonzalez et al., 2000), is provided in Fig. S2 in supplementary material. Briefly, slopes for successive windows of 15 points from the $\log(G/G_{max})$ *vs* V curve are determined and the values of the slopes reach a plateau at low values of G/G_{max} that represents the gating charge for the channel. Graphs illustrating the asymptotic behaviour of the gating charge (z_{lim}) values for all 12 channels are provided in Fig. S3 in supplementary material. Although it is also possible to measure directly the charge displacement associated with activation (Perozo et al., 1993), this method yields total charge movement, not just the charge movement that is directly coupled to channel opening (Sigg and Bezanilla, 1997).

Gibb's free energy values were calculated using the gating charge, determined as described above, and the V_{50} values obtained in Eqn 1:

$$\Delta G_0 = (z_{lim} F V_{50}). \quad (2)$$

For double mutant cycle analysis Gibb's free energy was compared to that of the wild-type channel:

$$\Delta\Delta G_0 = \Delta G_{0mut} - \Delta G_{0wt}. \quad (3)$$

Negative values of $\Delta\Delta G_0$ indicate that the equilibrium is shifted towards the open state, whereas positive values indicate increased stabilization of the closed state compared to the open state of the channel.

The significance of differences between electrophysiological parameters from different channels was assessed using a two-tailed t test.

Molecular modelling

The crystal structure of the $RatK_V1.2$ potassium channel (2A79.pdb) (Long et al., 2005) was used to create a complete model of the $RatK_V1.2$ channel, and this model was used as the basis for homology modelling of jShak1 in the open state. The crystal structure maps the coordinates for residues Cys32 to Gly131, Thr219 to Ala243 and Met288 to Thr421. Two unresolved chains are represented in the crystal structure by polyalanines. Chain C represents the T1-S1 linker and S1 helix, and chain D represents the S3 helix. Chains C and D are 52 and 21 residues long, respectively. The identity of the residues constituting chains C and D was determined using the known structural elements and secondary structure predictions from PredictProtein (Rost et al., 2004), on the complete primary sequence of $RatK_V1.2$ (NCBI accession no. P63142). The corresponding regions of the primary sequence were threaded onto the polyalanine backbones and the side chains were rebuilt using SwissPDBViewer (Guex and Peitsch, 1997; Peitsch, 1997; Peitsch et al., 1995; Schwede et al., 2003). The missing inter-helical loop regions of the voltage sensor were rebuilt using SwissPDB loop databases (Guex and Peitsch, 1997).

A homology model of jShak1 was constructed in SwissModel using the resolved residues of the $RatK_V1.2$ channel structure as a modelling template (Fig. S4 in supplementary material). The jShak1 sequence was aligned with 140 voltage-gated potassium channel

Table 1. Summarized fit parameters, including Gibb's free energy, for jShak1 S2/S4 mutants

Channel	*N*	V_{50} (mV)	Boltzmann slope (*b*)	z_{lim}	ΔG_0 (kJ mol^{-1})	$\Delta\Delta G_0$
jShak1wt	10	27.8±2.0	11.9±1.5	3.0±0.08	8.0±0.6	
N227D	5	21.8±3.5	16.0±1.6	2.8±0.4	5.9±1.3	–2.1±1.3
N227E	7	–8.6±3.9	16.0±2.5	2.3±0.3	–2.1±0.8	–10±1.3
QIF	7	–8.9±1.8	10.2±0.9	3.3±0.0	–2.9±0.4	–10.9±0.8
QIF-D	5	–14.1±3.0	16.9±3.9	2.8±0.08	–3.8±0.8	–11.7±0.8
QIF-E	6	–11.2±4.9	17.5±1.4	2.7±0.3	–2.9±1.3	–10.9±1.3
IFR	7	28.8±1.2	15.5±2.9	3.3±0.6	9.2±1.7	1.3±2.1
IFR-D	7	24.1±4.0	15.7±1.2	3.5±0.3	8.4±1.7	0.4±1.7
IFR-E	5	–4.8±5.7	16.9±1.1	2.3±0.2	–0.8±1.3	–8.8±1.3
RIF	8	55.0±2.5	10.1±0.5	2.8±0.3	15.1±2.1	7.1±2.1
RIF-D	5	55.6±1.7	10.9±1.2	2.7±0.2	14.7±0.8	6.7±1.3
RIF-E	8	40.4±2.4	13.9±1.7	3.1±0.4	12.1±1.7	4.2±1.7

sequences using MUSCLE v3.6 (Edgar, 2004a; Edgar, 2004b) and the pair-wise alignment of jShak1 and RatK_V1.2 was extracted. The alignment of jShak1 and RatK_V1.2 and corresponding secondary structure predictions (Rost et al., 2004) were used for the regions of jShak1 that were homologous to regions of RatK_V1.2. These regions were threaded onto the corresponding regions of the RatK_V1.2 crystal structure and the side-chains were rebuilt using SwissPDBViewer (Guex and Peitsch, 1997; Schwede et al., 2003). The inter-helix loops were rebuilt using SwissModel and SwissPDBViewer loop databases (Guex and Peitsch, 1997; Schwede et al., 2003). The resulting subunit model was energy minimized and refined to remove steric clashes. Symmetry information from the RatK_V1.2 crystal structure was used to derive the coordinates of the other three identical jShak1 subunits. The jShak1 channel model was tetramerized, with loop and interface regions refined. Finally, the model was energy minimized again to remove any residue clashes or irregularities at the subunit interfaces.

RESULTS

Relationship between V_{50}, gating charge and ΔG_0

In this set of channel mutants there was no significant correlation between V_{50} values and slope factors (r^2=0.34), or between V_{50} values and gating charge (z_{lim}) values calculated by the limiting slope method (r^2=0.076). There was also no correlation between the Boltzmann slope factors and z_{lim} values (r^2=0.077), which illustrates the importance of using a rigorous method to determine true gating charge values, rather than assuming a simple two-state equilibrium and calculating a gating charge value from the Boltzmann slope factor. However, there was a strong correlation between the V_{50} and the ΔG_0 for the 12 channels (r^2=0.99).

The gating charges for the wild-type channel and the 11 mutant channels ranged from 2.3 to 3.5 with a mean of ~2.9 (Table 1). This is considerably lower than the typical estimate for the *Drosophila* Shaker channel (~12). However, the limiting slope analyses of the gating charge for each of these channels yielded a plateau value (Fig. S3 in supplementary material), indicating that these are accurate measurements of the amount of charge involved in the gating process.

S2 mutants

As has been observed for other K_V channels, *jShak1* can be stabilized in the open state through formation of a salt bridge between an acidic residue at position 227 in S2 and positively charged residues in S4. Replacing the neutral asparagine at position 227 with an acidic residue, aspartate, (N227D) had no significant effect on the V_{50} of activation (21.8 mV for N227D *vs* 27.8 mV for wild type, P=0.16), the Boltzmann slope factor (P=0.09) or gating charge (P=0.76) compared with the wild-type channel (Fig. 3A, Table 1). The N227D mutation did not alter the equilibrium between open and closed states, since $\Delta\Delta G_0$ is not significantly different from 0 (P=0.19; Table 1).

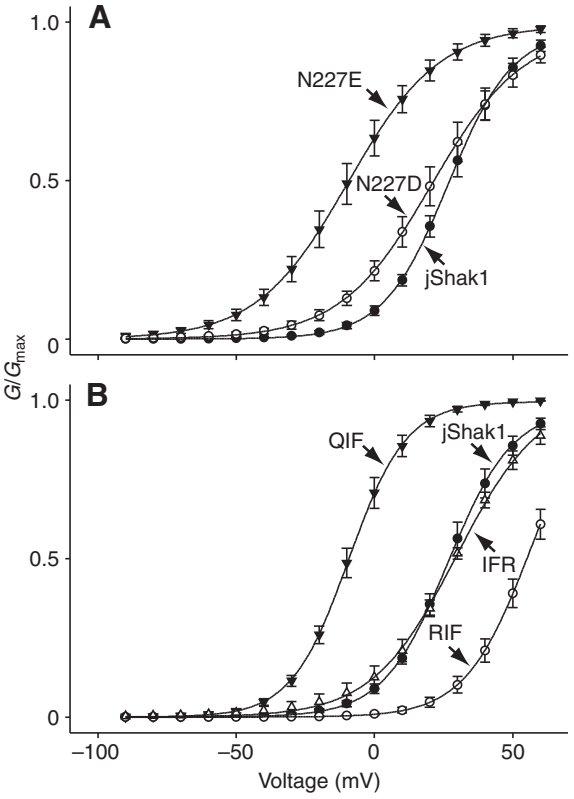

Fig. 3. Single mutations in the S2 helix and triplet insertions in the S4 helix modify steady-state activation properties. (A) The steady-state activation curve for jShak1 S2 mutants revealed that the N227E (inverted triangles) channels were activated at far more hyperpolarized potentials than wild-type channels (filled circles) and N227D mutant channels (open circles). The solid curve represents the fit to a Boltzmann function giving the voltage of half activation (V_{50}) and slope parameter (*b*) for each channel (error bars indicate s.e.m.). Fit parameters are summarized in Table 1. (B) The steady-state activation curve for jShak1 S4 insertion mutants revealed that insertion of the QIF motif (inverted triangles) to the N-terminal side of K294 shifted the activation curve in the hyperpolarized direction, the RIF insertion (open circles) shifted the activation curve in the depolarized direction, and the IFR insertion (open triangles) had no significant effect compared with wild-type channels (filled circles). The solid curve represents the fit to a Boltzmann function. Voltage of half activation (V_{50}) and Boltzmann slope factors (*b*) for each channel are summarized in Table 1 (error bars indicate s.e.m.).

The glutamate mutant (N227E), which differs from the N227D mutant by having an additional methylene group in the side chain of amino acid 227, caused the most significant shift of all of the single mutations examined. We observed a hyperpolarizing shift (by ~36 mV) of the V_{50} of activation to –8.6±3.9 mV (Fig. 3A, Table 1; $P=5.7\times10^{-7}$). This mutation had no effect on the Boltzmann slope factor ($P=0.19$). Although the difference in the gating charge is statistically insignificant ($P=0.06$), the low P value suggests that there may be a small underlying difference that could not be resolved with the available data. The N227E mutation substantially favoured the open state compared to the wild-type channel ($\Delta\Delta G_{0N227E}=-10$ kJ mol^{-1}; Table 1; $P=1.8\times10^{-7}$). Since this change in the gating charge was an insignificant decrease, it appears that this mutation acts primarily by stabilizing the open conformation, not by changing the nature of the motion of the S4 helix and the potential field during channel opening.

S4 mutants

Triplet Insertions

Although the effect of three-residue motifs inserted into S4 in the full-length channel were reported in an earlier study (Grigoriev et al., 1997), we have now characterized these mutations in the N-truncated channel to provide more accurate measures of V_{50}, slope factor and gating charge that can be compared to the values measured for other channel mutants that were also constructed as N-truncated channels. Although the slope values were similar to the previously published values, the V_{50} values differed noticeably from those previously reported for the N-inactivating channel (Fig. 3B, Table 1). The differences can be attributed to the errors arising from calculating conductance from peak current using an estimated potassium ion reversal potential (Grigoriev et al., 1997) as compared with directly measuring conductance from tail currents, as in this study.

The QIF mutation (Fig. 3B) shifts the channel behaviour to favour the open state relative to the wild-type channel ($\Delta\Delta G_{0QIF}=-10.9$ kJ mol^{-1}, $P=1.5\times10^{-9}$). The gating charge of this mutant is slightly greater than that for the wild-type channel (3.3 *vs* 3.0, $P=5.7\times10^{-4}$), in spite of the fact that the third arginine in S4 has been converted to an uncharged glutamine residue. The IFR insertion mutant does not significantly affect ΔG_0 ($P=0.5$), whereas the RIF insertional mutant shifts the channel towards the closed state relative to the wild-type channel ($\Delta\Delta G_0=7.1$ kJ mol^{-1}; $P=0.0035$; Fig. 3B, Table 1), and both the mutations have gating charges

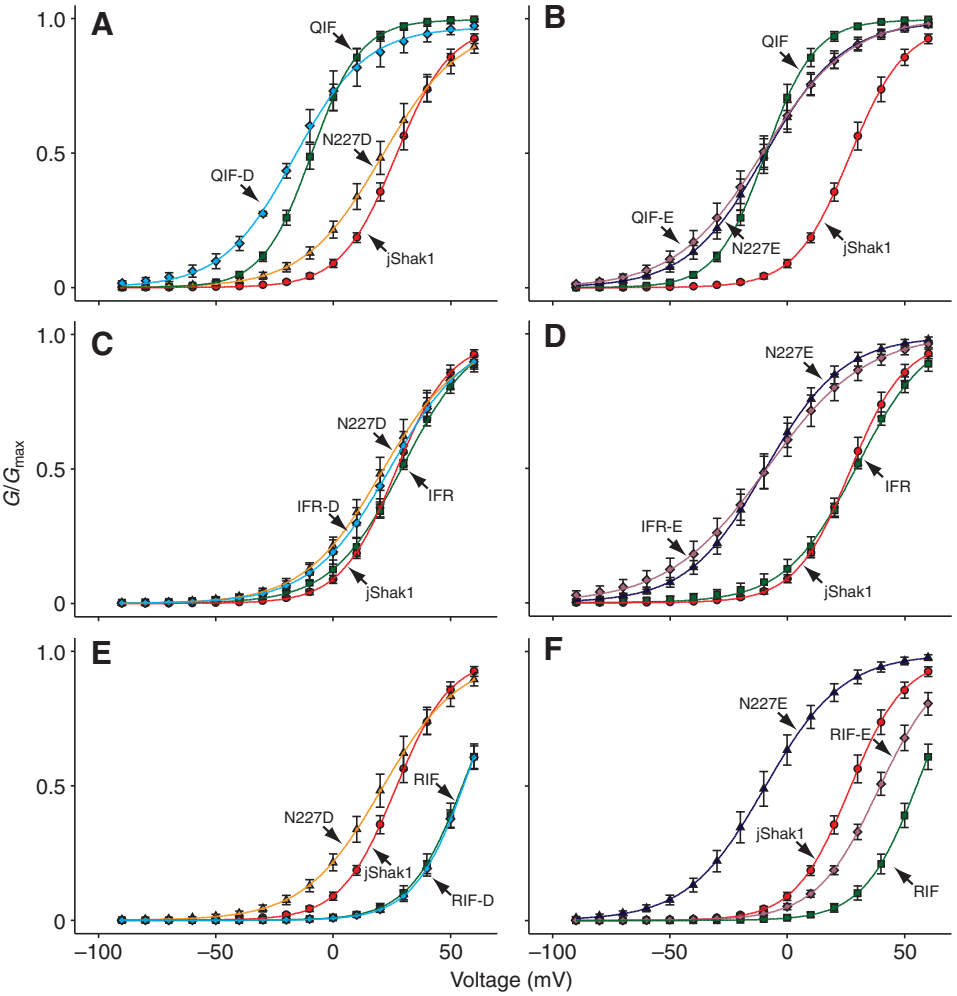

Fig. 4. The effects of combining S2 point mutations and S4 insertional mutations on steady-state activation properties. In all panels the wild-type jShak1 channel is indicated by the red circles, the S2 single mutants are indicated by triangles, the S4 insertion mutants are indicated by squares and the double mutants are indicated by diamonds. (A,C,E) The effect of combining the N227D mutation with the S4 triplet insertions in the double mutant channels. (B,D,F) The effect of combining the N227E mutation with the S4 triplet insertions in the double mutant channels. The solid curve represents the fit to a Boltzmann function. Voltage of half activation (V_{50}) and Boltzmann slope factors (b) for each channel are summarized in Table 1 (error bars indicate s.e.m.). (A) The effect of the N227D mutation in the S2 helix in combination with the QIF insertion mutation in S4 is similar to its effect on the wild-type channel. There appears to be a slight shift in slope factor and V_{50}, but the effect is not statistically significant. (B) The steady-state activation curve for the QIF-E double mutant (pink diamonds), the single QIF mutant (green squares), and the N227E point mutant (black triangles) were all shifted leftward approximately the same amount relative to the wild-type channel (red circles), but had different slopes, although the differences were not statistically significant. (C) The steady-state activation curves for the IFR-D double mutant (turquoise diamonds), the single mutant N227D (orange triangles), IFR insertion alone (green squares) were not significantly different from the wild-type channel (red circles). (D) The steady-state activation curve for the IFR-E double mutant (pink diamonds) was shifted in a hyperpolarized direction relative to the IFR mutant alone (green squares) and the wild-type channel (red circles) and had a similar V_{50} of activation to that of the N227E single mutant (blue triangles), but with a larger slope factor, b. (E) The steady-state activation curve for the RIF-D double mutant (turquoise diamonds) was shifted in a depolarized direction relative to the single N227D mutant (orange triangles), to the same extent that the RIF mutant (green squares) was shifted relative to the wild-type channel (red circles). (F) The steady-state activation curve for the RIF-E double mutant (pink diamonds) was shifted in a depolarized direction relative to the wild-type channel (red circles), which was in the opposite direction to the shift for the N227E single mutant (black triangles). The RIF-E double mutant is also shifted in the hyperpolarizing direction relative to the RIF mutant alone (green squares).

Table 2. Double mutant cycle analysis: $\Delta\Delta G_0$ for single mutations and double mutations

S4 mutants / S2 mutants		N227E Single mutant	N227E Sum single mutations	N227E Double mutant	N227E Difference*	N227D Single mutant	N227D Sum single mutations	N227D Double mutant	N227D Difference*
	$\Delta\Delta G_0$	–10				–2.1			
QIF	–10.9		–20.9±1.3	–10.9	10±2.1		–13±1.7	–11.7	1.3±2.1
IFR	1.3		–8.7±2.1	–8.8	–0.1±2.5		–0.8±2.5	0.4	1.2±2.9
RIF	7.1		–2.9±2.5	4.2	7.1 ±2.9		5.0±2.5	6.7	1.7±2.9

*Difference was calculated: Difference = $\Delta\Delta G_{0\text{double}} - (\Delta\Delta G_{0\text{singleS2}} + \Delta\Delta G_{0\text{singleS4}})$.

indistinguishable from that of the wild-type channel (P=0.58 and P=0.66, respectively).

S2-S4 double mutants

QIF mutations

When the N227D mutation was combined with the QIF addition (Fig. 4A), the double mutant, QIF-D, showed a further 5.2 mV leftward shift in activation (Table 1), and a slightly lower gating charge of 2.8 compared with 3.3 (P=5.7×10^{-5}) relative to the QIF mutation alone (Table 1). The stabilization of the open state by the QIF-D double mutation was not significantly different from the sum of the effects of the QIF and N227D mutations individually ($\Delta\Delta G_{0\text{QIF-D}}$=–11.7 kJ mol^{-1} compared with $\Delta\Delta G_{0\text{QIF}}+\Delta\Delta G_{0\text{N227D}}$= –13 kJ mol^{-1}; P=0.61; Table 2). This similarity in $\Delta\Delta G_0$ for the double mutant compared to the sum of the $\Delta\Delta G_0$ values for the single mutants indicates that the N227D mutation in S2 and the QIF mutation in S4 act independently and therefore additively on the channel.

The double mutant QIF+N227E (QIF-E) did not shift the V_{50} of activation, the gating charge or the $\Delta\Delta G_0$ significantly relative to the QIF mutant alone, (Fig. 4B; P=0.66, P=0.065, P=0.96, respectively). Gibb's free energy calculations show that QIF-E favoured the open state compared with the wild-type channel (P=2.7×10^{-6}). However, the sum of Gibb's free energies for the single mutants was more negative than that observed in the double mutant (P=4.6×10^{-4}), indicating that the combined QIF and the N227E mutations antagonized each other's independent abilities to stabilize the open state.

IFR mutations

The double mutant combining IFR+N227D (IFR-D) had no significant effect on the V_{50} of activation relative to that of the wild type (Fig. 4C; P=0.43). This double mutant favours the open state of the channel to the same extent as the wild-type channel (P=0.88). This effect was equivalent to the summed effect of the single mutations (P=0.76).

The V_{50} of activation for the double mutant IFR+N227E (IFR-E) was shifted in the hyperpolarized direction by approximately 33.6 mV compared with the IFR mutant alone (Fig. 4D; P=1.9×10^{-4}). Notably, the Gibb's free energy value for the IFR-E double mutation did not differ from the sum of the free-energy values for independent IFR and N227E mutations (P=0.86) indicating that these mutations in S2 and S4 acted independently in the double mutant.

RIF mutations

The double mutant RIF+N227D (RIF-D) failed to alter either the V_{50} or gating charge compared with the single RIF mutant (Fig. 4E, Table 1; P=0.84 and P=0.79, respectively). Combining the RIF and N227D mutations did not modify the channel's equilibrium more than would be expected from the sum of the independent single mutations (P=0.57; Table 2), indicating that the two mutations are acting independently.

In comparison, the RIF+N227E (RIF-E) mutant had a hyperpolarizing shift of 14.6 mV compared with the RIF mutant alone (Table 1; Fig. 4F; P=8.6×10^{-4}). This double mutation did not significantly affect the gating charge (P=0.52). Double mutant cycle analysis shows that the two mutations did not act independently ($\Delta\Delta G_{0\text{RIF-E}}$=4.2 kJ mol^{-1} compared with $\Delta\Delta G_{0\text{RIF}}+\Delta\Delta G_{0\text{N227E}}$= –2.9 kJ mol^{-1}; Table 2; P=0.03), since the two mutations interfered with each other so as to move the equilibrium towards the closed state.

Homology modelling of jShak1 on the RatK$_V$1.2 template

The open-state jShak1 homology model gives a continuous representation of the intracellular domain and transmembrane domain of the channel, minus the N terminus and C terminus. Loop regions missing from the original RatK$_V$1.2 crystal structure have been rebuilt from loop databases to give a continuous model of the transmembrane domain, from the start of the T1-S1 linker to the end of the S6 helix. Analysis of the Ramachandran plot for the hybrid K$_V$1.2 structure shows that 99% of residues were in favourable regions of the plot, compared with 94% of residues in favourable regions in the jShak1 model. PROCHECK and WHAT IF protein structure checks were performed on the open-state homology model and the original K$_V$1.2 crystal structure. The results showed that models were of comparable quality to the template crystal structure. The backbone root-mean-squared deviation (RMSD) between the jShak1 open-state homology model and the RatK$_V$1.2 crystal structure was 0.13 Å.

It is important to note that the RatK$_V$1.2 channel was crystallized in the absence of an intact membrane (i.e. equivalent to a 0 mV transmembrane potential), and so it represents the open conformation of the channel since the V_{50} for RatK$_V$1.2 has been reported to be –17 mV (Scholle et al., 2000).

Fig. 5A shows the alignment of the S3-linker-S4 portion of the two structures. The RatK$_V$1.2 linker is large and flexible and includes a helical region, as predicted from the mutagenesis analysis by Mathur and others (Mathur et al., 1997). The jShak1 linker is short, nearly the length of a fully extended polypeptide, and thus appears to anchor the C-terminal end of S3 to the N-terminal end of S4 during channel transitions between the open and closed state. The strong similarities in the structures of the S4 helices and the L4-5 linkers in the open states of these channels is illustrated in Fig. 5B. When the membrane is depolarized, translocation of the S4 helix is coupled to lateral movement of the L4-5 segment that pulls the intracellular ends of the S5 and S6 helices apart, opening the activation gate, allowing K^+ flow through the pore. Because of this

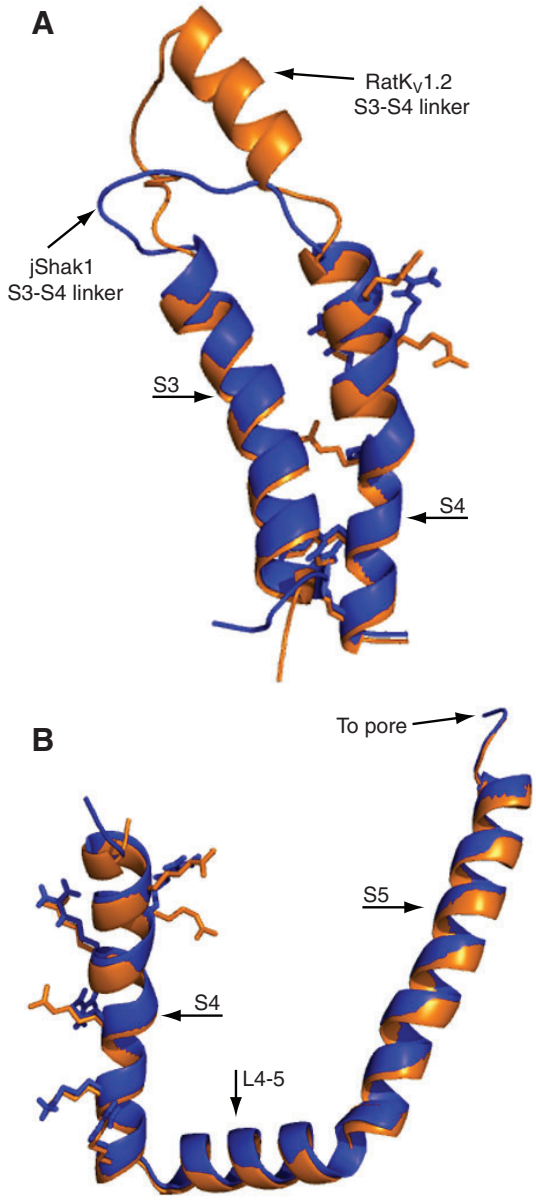

Fig. 5. Homology models of the structural constraints in jShak1 based on the crystal structure of RatK$_V$1.2. (A) Overlay of S3 and S4 showing the extremely short three amino acid S3-S4 linker which anchors the C-terminal end of S3 closely to the N-terminal end of S4 in jShak1 during gating transitions. The homology model of jShak1 (blue) is placed over the model of RatK$_V$1.2 (gold). The basic residues in S4 are illustrated as side-chain sticks, and transmembrane helices are labelled. (B) Overlay of the highly conserved S4-S5 linker (L4-5) that is conserved in both RatK$_V$1.2 (gold) and jShak1 (blue). The L4-5 linker couples the translocation of the voltage sensor to the opening of activation gate. This conserved mechanism suggests that length insertions in the short S4 of *jShak1* should move residues extracellularly rather than modify the amphipathic packing of L4-5.

essential function, it is expected that the three mutations that insert a tripeptide into the S4 helix will distort the conformation of the channel by displacing the N terminus of the S4 helix in an outward (extracellular) direction, rather than disrupting the conformation of L4-5. The length, shape and conformation of the S3-S4 linker has been shown to affect voltage sensitivity (Gonzalez et al., 2001; Mathur et al., 1997), suggesting that in jShak1 increasing the length of the S4 helix might affect voltage sensitivity by creating a voltage sensor with greater internal tension that alters the equilibrium between the open and closed state, independent of charge content.

The alignment of the S2 helices (Fig. 6A) illustrates the positional equivalence of RatK$_V$1.2 E226 and jShak1 N227 and of RatK$_V$1.2 E236 and jShak1 E237, as shown in the alignment in Fig. 1B. The alignment of the S4 helices shows that the alignment of the S4 helices of RatK$_V$1.2 and jShak1 are consistent with the alignment shown in Fig. 1B, with the exception that the SML tripeptide at the N-terminal end of the jShak1 S4 is part of the helix, and not part of the connecting linker (Fig. 6B).

DISCUSSION

Perturbation analysis compares the difference in free energy between the open and closed states of the wild-type channel with that of the mutant channels (Hong and Miller, 2000; Li-Smerin et al., 2000; Monks et al., 1999; Perozo, 2000). In double mutant cycle analysis the $\Delta\Delta G_0$ values for two, independent single mutations are compared with the observed $\Delta\Delta G_0$ value for the double mutant channel. If the difference between the double mutant and the summed $\Delta\Delta G_0$ for the single mutants is zero [$\Delta\Delta G_{0\text{double}}-(\Delta\Delta G_{0\text{mut1}}+\Delta\Delta G_{0\text{mut2}})=0$], then the single mutations are acting independently in the double mutant channel (Horovitz, 1996). Conversely, if there is a difference between the double mutant and the sum of the single mutations [$\Delta\Delta G_{0\text{double}}-(\Delta\Delta G_{0\text{mut1}}+\Delta\Delta G_{0\text{mut2}})\neq 0$] then the residues at the two positions are energetically coupled, either through direct or indirect interactions. Differences in $\Delta\Delta G_0$ provide a measure of the strength of pair-wise interactions between sites of mutations (Horovitz, 1996). In our study, if the difference between $\Delta\Delta G_{0\text{double}}$ and $\Delta\Delta G_{0\text{mut1}}+\Delta\Delta G_{0\text{mut2}}$ was greater than zero then the interaction between the two residues tended to stabilize the closed conformation whereas a difference less than zero indicated that the interaction between the two mutated residues tended to favour the open conformation.

jShak1 has a number of structural features that make it useful for probing structural interactions involved in stabilizing the open and closed conformations of VKCs. The S2 transmembrane helix of jShak1 contains a single acidic residue (E237) that is conserved in other K$_V$1 channels, but lacks a second acidic residue that is present in most other K$_V$1 channels, being an asparagine in jShak1 (N227) (Fig. 1B). The S4 voltage sensor is shorter by a single triplet motif than other K$_V$1 channels, containing 6 basic residues corresponding to R365-R380 in *Drosophila* Shaker (Fig. 1B). Modelling indicates that the length of S4 is similar to other K$_V$1 channels, but the Ser-Met-Val (SML) amino acid sequence replaces the N-terminal basic motif, so although the voltage-sensing element is shorter, the total S4 helix is similar in length to that in other channels. Finally, the S3-S4 linker in the wild-type jShak1 channel is the shortest reported in any K$_V$ channel, being composed of only three amino acids. This constrains the intramolecular distance between the S3 and S4 helices, such that small modifications to amino acid length (aspartic acid *vs* glutamic acid) and relative packing in this region (IFR *vs* RIF) can be observed to directly influence the internal energetics of the channel. All of the jShak1 mutants, including those with the tripeptide insert, open in response to voltage, demonstrating that both the voltage sensor and linker are able to move during activation. However, changes in the length, shape and conformation of the S3-S4 linker have been shown to affect voltage sensitivity in *Drosophila* Shaker (Mathur et al., 1997).

We determined a relatively small (~2.9 e) gating charge for jShak1 and all of its mutants. This is much smaller than the total gating charge determined for the *Drosophila* Shaker channel (~12–13 e),

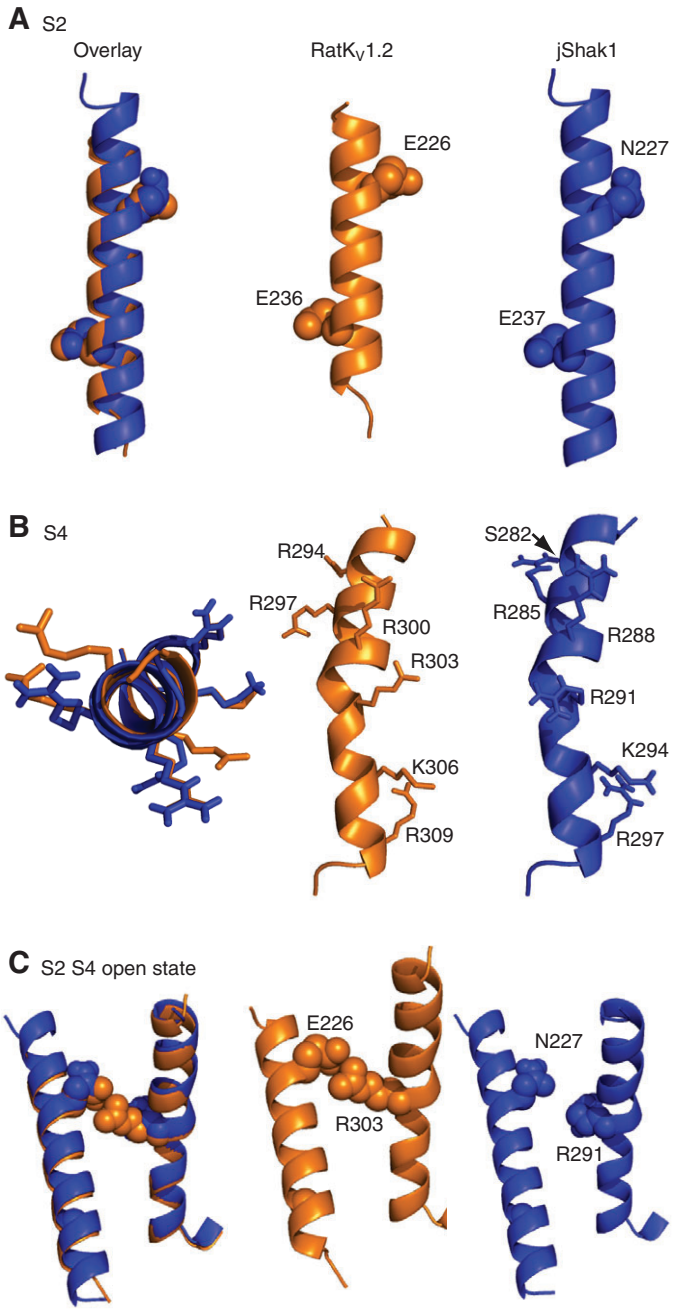

Fig. 6. The S2 and S4 of jShak1 lack favourable electrostatic interactions in the open state that are present in most other K_V1 channels. (A) A structural overlay of S2 transmembrane domains of Rat$K_V1.2$ (gold) and jShak1 (blue) showing the homology of positions of E226 (Rat$K_V1.2$) to N227 (jShak1) and E236 (Rat$K_V1.2$) to E237 (jShak1), respectively. The short non-charged side-chain of N227 prevents favourable electrostatic interactions with S4 residues in the open conformation that can be recovered with mutations to glutamate (N227E). (B) A structural overlay of S4 showing relative locations of the S4 basic residue side chains in Rat$K_V1.2$ (gold) and the shortened S4 of jShak1 (blue). The periodicity and side-chain location of the arginine residues between the channels is preserved at the C-terminal end of the helix. Specifically, positions K306/R309 in Rat$K_V1.2$ overlay K274/R377 in Rat$K_V1.2$. (C) Homology model of the interactions between S2 and S4 residues in the open conformation of the channel illustrating the favourable salt bridge interactions between E226 and R303. The N227 residue in jShak1 (blue) does not form a salt bridge with R291, whereas E226 shows a strong interaction with R303 in Rat$K_V1.2$ (gold).

but other channels, e.g. *Drosophila* Shab (~7.5 e) (Islas and Sigworth, 1999) and human herg (~6 e) (Zhang et al., 2004) show that a wide range of gating charge values can support physiologically relevant voltage sensitivity. The number of gating charges is a function of the total displacement of the charged residues in the transmembrane potential field, so a lower gating charge could arise from (1) fewer charges in the voltage sensor, (2) less displacement of the voltage sensor charges through the potential field or (3) a wider, more diffuse potential field such that the charges traverse a smaller proportion of the potential field. It is noteworthy that a synthetic mutation that shortens the loop connecting S3 and S4 in the *Drosophila* Shaker channel causes a decrease in gating charge from 12 e to approximately 5 e (Gonzalez et al., 2000); as noted above, the *jShak1* channel has a very short loop connecting S3 and S4.

The energy required for channel opening is a function of the product of the V_{50} and the number of charges that move during the opening transition. Thus, the mutations that are described here could have caused changes in the energy required for opening through two distinct effects; changing the amount of charge translocated through the membrane potential field, and changing the internal energy difference between the open and closed state. The gating charge values were changed little by the various mutations and there was little correlation between the values of the gating charges and the V_{50} values; however, the V_{50} values were highly correlated with the ΔG_0 values. Thus, the difference between the internal energies of the open and closed states of the channels is the primary factor that is affecting V_{50} in this set of mutations. The mutations are not appreciably affecting the underlying mechanics of the gating process.

Effects of single mutations in S2

Substitution of N227 with aspartate did not have a significant effect on the channel, whereas substitution of N227 with glutamate shifted the channel equilibrium strongly toward the open state. This indicates that simply converting the neutral asparagines to negatively charged aspartate at this position does not lead to formation of a strong salt bridge, but that the increased length of an additional methylene group in the side chain (a length of ~1.5 ångströms) in the glutamate residue, does lead to significant stabilization. However, the energy difference between the wild-type and the N227E mutant is only $-10.5\,kJ\,mol^{-1}$, approximately half of what would be expected from a fully formed salt bridge (Kumar and Nussinov, 1999). The most straightforward interpretation of this result is that the S2 and S4 helices in jShak1 are strongly constrained from moving towards each other, thus physically constraining the extent of interactions between the side-chains of adjacent helices. The additional length in the N227E side-chain allows the negatively charged carboxylate group to be closer to positively charged S4 residues in the open state, thus yielding a more stable open state than the shorter side-chain of the N227D mutation, but still not at the energy minimum for a fully formed salt bridge.

Effects of S4 triplet insertion mutations

Insertion of RIF upstream of K294 produced a channel in which the energy difference between the closed state and the open state was $+15.1\,kJ\,mol^{-1}$, which is $+7.1\,kJ\,mol^{-1}$ more than for the wild-type channel. We hypothesize that this difference can be attributed to increased resistance to translocation of the longer S4 helix in the RIF mutant, because of constraint by the short S3-S4 linker.

Insertion of QIF upstream of K294 produced a channel in which the energy difference between the closed state and the open state

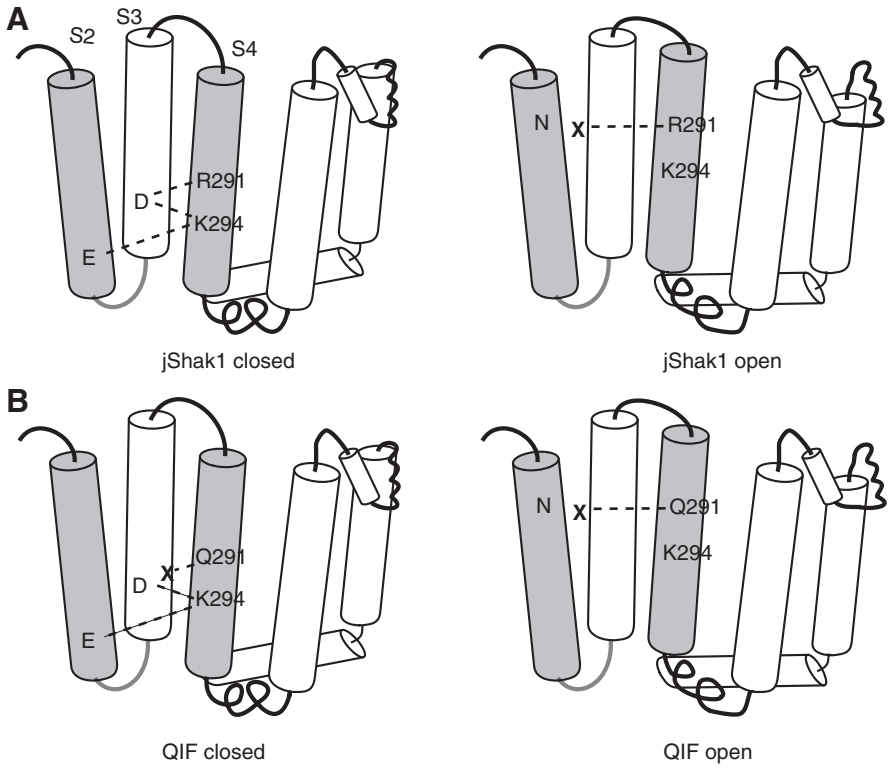

Fig. 7. Schematic of interactions occurring between the S2 and S4 helices in the open and closed states in the jShak1 and QIF channels. (A) jShak1 in closed state (left) is stabilized by charge-pair interactions between positively charged R291 and K294 on the S4 helix and negatively charged E237 on S2 and D260 on S3. In the transition to the open state the interactions between R291 and the two acidic residues are broken and R291 comes into proximity to N227, which is uncharged. In the N227E mutant the open state is stabilized by the R291–E227 charge interaction, shifting the equilibrium toward the open state. (B) In the QIF mutation, where glutamine occupies the position normally taken by R291, there are no charge interactions between the glutamine residue, E237 and D260 to stabilize the closed state, so the equilibrium is shifted towards the open state. Replacement of N227 with acidic residues does not increase stabilization of the open state because the glutamine does not interact strongly with the acidic residues.

was –2.9 kJ mol^{-1}, which is 10.9 kJ mol^{-1} less than for the wild-type channel. Since the effect of a longer S4 helix should be the same in QIF and RIF, the implication is that the glutamine residue in QIF is causing an approximately 18 kJ mol^{-1} destabilization of the closed state relative to the open state. This energy difference is quantitatively similar to the typical stabilizing energy of a salt bridge (Kumar and Nussinov, 1999). Since the homologous residue in *Drosophila* Shaker is known to interact with charged residues in S2 and S3 in the closed state (Papazian et al., 1995), this energy difference appears to be due to the absence of a salt bridge formed between the inserted glutamine residue and one or both of residues E237 and D260 (see Fig. 1) in the closed state of the QIF mutant. Thus, stabilization of the closed state due to the increased length of S4 is more than offset by the loss of charge interactions that also stabilize the closed state.

The energy difference between open and closed states in the IFR mutant is not significantly different from that of the wild-type channel. This can be compared to a difference of +7.1 kJ mol^{-1} for the RIF mutant. In the IFR channel the K294 residue has been displaced approximately one helical turn in the extracellular direction. It appears that the presence of an arginine in place of the lysine in the IFR mutant, and the replacement of the adjacent arginine with a lysine causes a net destabilization of the closed state relative to the open state. This could be due to several factors, possibly in combination, including (1) a weaker interaction between lysine and residues E237 and D260 than between arginine and those residues in the closed state, (2) a stronger interaction between lysine and N227 than between arginine and N227 in the open state, and (3) a combination of small energetic differences from changes in packing of the uncharged amino acids.

Interactions between mutations in S2 and S4

There is no significant difference in ΔG_0 among the leftward-shifted channels, QIF, QIF-D and QIF-E. This suggests that the wild-type, N227E or N227D S2 helices had comparable interactions with the S4 helix. This seems reasonable since the arginine that normally interacts with the amino acid at position 227 has been replaced by glutamine, preventing a salt bridge forming between these two residues in the open state. However, the sum of the single $\Delta\Delta G_0$ for QIF and N227E mutations predicted a greater stabilization of the open state ($\Delta\Delta G_{0\mathrm{QIF}}+\Delta\Delta G_{0\mathrm{N227E}}$=–21 kJ mol^{-1}) than was observed in the double mutant channel ($\Delta\Delta G_{0\mathrm{QIF\text{-}E}}$=–10.9 kJ mol^{-1}) indicating an interfering interaction between the two mutations, whereas a simple additive interaction was observed for the QIF-D double mutant. Since the difference between the QIF-D and QIF-E double mutants is that the side-chain of the acidic residue at position 227 has one more methylene group in the glutamate than in the aspartate, this may indicate that the S2 and S4 helices are packed so close together that the steric interference caused by the additional methylene group causes more destabilization than is gained by any polar interaction between the glutamate carboxyl group at position 227 and the glutamine side chain. This is in contrast to the effect of the N227E mutation on the wild-type channel, suggesting that the addition of the QIF motif to the S4 helix has caused it to be packed much closer to the S2 helix in the open state than is the case for the wild-type S4 helix.

In the IFR double mutants, the presence of acidic S2 residues also favoured the open conformation of the channel. The IFR-E mutation, with the longer glutamate side-chain shifted the half activation voltage leftward by ~29 mV as compared to the IFR-D mutation, which had an insignificant effect when compared with the wild type. Double mutant cycle analysis showed that both the N227D and the N227E mutation act independently with the IFR mutation. This means that insertions of triplet motifs at different locations in the S4 helix are having different effects on the way that S4 is interacting with S2.

Although the RIF insert in S4 shifted the equilibrium to favour the closed state, and the RIF-N227D double mutant was functionally

indistinguishable from the RIF mutant alone, the RIF-N227E mutant, with the longer acidic residue side-chain, shifted the equilibrium towards the open state compared with the RIF single mutant alone. The RIF mutation effect was independent of the N227D mutation, but the RIF mutation had an interfering interaction with the N227E mutation, similar to, but smaller in magnitude than, the interfering interaction between the QIF mutations and the N227E mutation.

These results can be explained in terms of three factors that affect the relative stability of the open and closed states, and hence the voltage sensitivity, of the channel (Fig. 7). First, the insertion of three amino acids in the S4 helix tends to stabilize the closed state relative to the open state. Since the interaction of S4 with the S4/S5 linker is conserved and central to the mechanism of channel opening and the S3/S4 linker is so short that it restricts the relative motion of S3 and S4, we infer that the increased length of S4 is creating internal constraint on S4 that resists its motion in the transition from the open to the closed state, thus causing the rightward shift in voltage sensitivity.

The second factor that affects the relative stability of the open and the closed state is the interaction between the amino acid residue at position 291 and the two acidic residues in S2 and S3 in the closed state (Papazian et al., 1995). In the case of the QIF insertion mutant, stabilization of the closed state is offset by the fact that the neutral glutamine residue is in a location that is normally occupied by a positively charged arginine residue. In the wild-type channel this arginine residue interacts with the acidic residues in S2 and S3, helping to stabilize the closed conformation (Fig. 7A). However, in the QIF mutant the substituted glutamine residue cannot form these charge interactions (Fig. 7C), thus destabilizing the closed state and causing a significant leftward shift in the V_{50} value, in spite of the constraint on movement caused by the short S3/S4 linker.

The third factor affecting the relative stability of the open and closed conformations is the interaction between the residue at position 291 and the residue at position 227 in the open state. In the case of the wild-type S4 (Fig. 7B), and the RIF and IFR insertions in S4, mutation of N227 to aspartate and glutamate both decrease the ΔG_0 of the channels, although to different extents. In all three cases the N227E mutation has a larger effect, probably as a result of the side chain being one methylene group longer than that of aspartate, thus allowing the positive charge at position 291 and the negative charge at position 227 to interact more strongly. In the case of the QIF double mutations, the N227D mutation yields a small decrease in ΔG_0 but the N227E mutation yields no change over the QIF mutant alone. We hypothesize that this is because of a steric crowding effect of the longer glutamate side-chain with the glutamine at position 291, which is not offset by any electrostatic energy gain, since there is no positive charge on the glutamine side chain (Fig. 7D).

In the absence of high-resolution structures of the ion channel of interest, homology models provide a three-dimensional map of a protein. They are structural predictors, which are highly dependent on the accuracy of the underlying sequence alignment and, as such, require progressive refinement as new results become available. In the case of the jShak1 open-state homology model, secondary structure predictions and loop database searches were used to bridge the gaps in the RatK_V1.2 template structure, allowing the development of a more complete homology model.

A homology model, like the crystal structure on which is based, represents a single, state-dependent snapshot of jShak1. Although the open-state jShak1 model described here is a true homology model, there is no crystal structure of a voltage-gated channel in a closed state on which to base a comparable model.

Thus, to investigate and understand the details of the molecular mechanics of the transition between closed to open states in responses to changes in membrane potential it is valuable to use the structural model as a heuristic framework for formulating hypotheses that can be tested by mutagenesis. In turn, electrophysiological characterization of well-designed mutant channels provides dynamic data that can inform subsequent rounds of modelling and hypotheses about the detailed molecular mechanisms of channel opening and closing.

The model of the S2 and S4 helices (Fig. 6C) illustrates a basis for the difference between the wild-type and N227E mutant of jShak1. In the wild-type channel (Fig. 6C) the N227 residue is not in close proximity to any of the basic residues of S4, whereas in the RatK_V1.2 model (Fig. 6C) the glutamate residue (E226) at the position homologous to E227 in jShak1 is very close to one of the arginine residues (R303) in the S4 helix; this interaction would be expected to stabilize the open configuration of the channel, by virtue of a salt bridge, and thus yield a V_{50} value considerably more hyperpolarized than that for a channel without an acidic residue in that position in S2. In this homology model, the channel is in the open conformation, and the residues that are thought to stabilize the closed state by forming salt bridges are not in close proximity. It is clear that the process of channel closing will require rotation and translocation of all three helices to form the predicted interaction network between residues E237, D260 and positive residues in S4 of jShak1, as described for *Drosophila* Shaker (Papazian et al., 1995).

LIST OF ABBREVIATIONS

b	Boltzmann slope factor
F	Faraday constant
G	conductance
I	current
V_{50}	voltage at which conductance is 50% of maximum conductance
VKC	voltage-gated potassium channel
z_{lim}	gating charge as estimated by limiting slope method, in units of single electron charge
ΔG	difference in standard Gibb's free energy

This study was supported by a grant from CIHR (MOP-62685) to A.N.S. and W.J.G. M.L.O. is a CIHR postdoctoral fellow. Student support was provided to T.L.K. through an NSERC PGS-D. The homology modelling was done in Dr D. Peter Tieleman's group in the Department of Biological Science, University of Calgary. We thank him for the use of his facilities and resources, which are funded by AHFMR and CIHR.

REFERENCES

Ahern, C. A. and Horn, R. (2005). Focused electric field across the voltage sensor of potassium channels. *Neuron* **48**, 25-29.

Almers, W. (1978). Gating currents and charge movements in excitable membranes. *Rev. Physiol. Biochem. Pharmacol.* **82**, 96-190.

Ausubel, F. M., Brent, R., Kingston, R. E., Moore, D. D., Seidman, J. G., Smith, J. A. and Struhl, K. (1987). *Current Protocols in Molecular Biology*. New York: John Wiley.

Baker, O. S., Larsson, H. P., Mannuzzu, L. M. and Isacoff, E. Y. (1998). Three transmembrane conformations and sequence-dependent displacement of the S4 domain in shaker K^+ channel gating. *Neuron* **20**, 1283-1294.

Bezanilla, F., Perozo, E. and Stefani, E. (1994). Gating of Shaker K^+ channels: II the components of gating currents and a model of channel activation. *Biophys. J.* **66**, 1011-1021.

Bouchard, C., Price, R. B., Moneypenny, C. G., Thompson, L. F., Zillhardt, M., Stalheim, L. and Anderson, P. A. (2006). Cloning and functional expression of voltage-gated ion channel subunits from cnidocytes of the Portuguese Man O' War *Physalia physalis*. *J. Exp. Biol.* **209**, 2979-2989.

Chanda, B., Asamoah, O. K., Blunck, R., Roux, B. and Bezanilla, F. (2005). Gating charge displacement in voltage-gated ion channels involves limited transmembrane movement. *Nature* **436**, 852-856.

Connor, J. A. and Stevens, C. F. (1971a). Inward and delayed outward membrane currents in isolated neural somata under voltage clamp. *J. Physiol.* **213**, 1-19.
Connor, J. A. and Stevens, C. F. (1971b). Prediction of repetitive firing behaviour from voltage clamp data on an isolated neurone soma. *J. Physiol.* **213**, 31-53.
Connor, J. A. and Stevens, C. F. (1971c). Voltage clamp studies of a transient outward membrane current in gastropod neural somata. *J. Physiol.* **213**, 21-30.
Durell, S. R., Shrivastava, I. H. and Guy, H. R. (2004). Models of the structure and voltage-gating mechanism of the shaker K^+ channel. *Biophys. J.* **87**, 2116-2130.
Edgar, R. C. (2004a). MUSCLE: a multiple sequence alignment method with reduced time and space complexity. *BMC Bioinformatics* **5**, 113.
Edgar, R. C. (2004b). MUSCLE: multiple sequence alignment with high accuracy and high throughput. *Nucleic Acids Res.* **32**, 1792-1797.
Gonzalez, C., Rosenman, E., Bezanilla, F., Alvarez, O. and Latorre, R. (2000). Modulation of the Shaker K(+) channel gating kinetics by the S3-S4 linker. *J. Gen. Physiol.* **115**, 193-208.
Gonzalez, C., Rosenman, E., Bezanilla, F., Alvarez, O. and Latorre, R. (2001). Periodic perturbations in Shaker K^+ channel gating kinetics by deletions in the S3-S4 linker. *Proc. Natl. Acad. Sci. USA* **98**, 9617-9623.
Grigoriev, N. G., Spafford, J. D., Gallin, W. J. and Spencer, A. N. (1997). Voltage sensing in jellyfish Shaker K^+ channels. *J. Exp. Biol.* **200**, 2919-2926.
Guan, D., Lee, J. C., Higgs, M. H., Spain, W. J. and Foehring, R. C. (2007). Functional roles of KV1 channels in neocortical pyramidal neurons. *J. Neurophysiol.* **97**, 1931-1940.
Guex, N. and Peitsch, M. C. (1997). SWISS-MODEL and the Swiss-PdbViewer: an environment for comparative protein modeling. *Electrophoresis* **18**, 2714-2723.
Guy, H. R., Durell, S. R., Warmke, J., Drysdale, R. and Ganetzky, B. (1991). Similarities in amino acid sequences of Drosophila eag and cyclic nucleotide-gated channels. *Science* **254**, 730.
Hong, K. H. and Miller, C. (2000). The lipid-protein interface of a Shaker K(+) channel. *J. Gen. Physiol.* **115**, 51-58.
Horovitz, A. (1996). Double-mutant cycles: a powerful tool for analyzing protein structure and function. *Fold. Des.* **1**, R121-R126.
Hoshi, T., Zagotta, W. N. and Aldrich, R. W. (1990). Biophysical and molecular mechanisms of Shaker potassium channel inactivation. *Science* **250**, 533-538.
Huang, Q. Q., Harvey, C. M., Paterson, A. R., Cass, C. E. and Young, J. D. (1993). Functional expression of Na(+)-dependent nucleoside transport systems of rat intestine in isolated oocytes of Xenopus laevis. Demonstration that rat jejunum expresses the purine-selective system N1 (cif) and a second, novel system N3 having broad specificity for purine and pyrimidine nucleosides. *J. Biol. Chem.* **268**, 20613-20619.
Islas, L. D. and Sigworth, F. J. (1999). Voltage sensitivity and gating charge in Shaker and Shab family potassium channels. *J. Gen. Physiol.* **114**, 723-742.
Islas, L. D. and Sigworth, F. J. (2001). Electrostatics and the gating pore of *Shaker* potassium channels. *J. Gen. Physiol.* **117**, 69-89.
Jegla, T., Grigoriev, N., Gallin, W. J., Salkoff, L. and Spencer, A. N. (1995). Multiple Shaker potassium channels in a primitive metazoan. *J. Neurosci.* **15**, 7989-7999.
Kasten, M. R., Rudy, B. and Anderson, M. P. (2007). Differential regulation of action potential firing in adult murine thalamocortical neurons by KV3.2, KV1, and SK potassium and N-type calcium channels. *J. Physiol.* **584**, 565-582.
Kumar, S. and Nussinov, R. (1999). Salt bridge stability in monomeric proteins. *J. Mol. Biol.* **293**, 1241-1255.
Li-Smerin, Y., Hackos, D. H. and Swartz, K. J. (2000). alpha-helical structural elements within the voltage-sensing domains of a K(+) channel. *J. Gen. Physiol.* **115**, 33-50.
Long, S. B., Campbell, E. B. and Mackinnon, R. (2005). Crystal structure of a mammalian voltage-dependent Shaker family K^+ channel. *Science* **309**, 897-903.
Mathur, R., Zheng, J., Yan, Y. and Sigworth, F. J. (1997). Role of the S3-S4 linker in Shaker potassium channel activation. *J. Gen. Physiol.* **109**, 191-199.
Monks, S. A., Needleman, D. J. and Miller, C. (1999). Helical structure and packing orientation of the S2 segment in the Shaker K^+ channel. *J. Gen. Physiol.* **113**, 415-423.
Noda, M., Shimizu, S., Tanabe, T., Takai, T., Kayano, T., Ikeda, T., Takahashi, H., Nakayama, H., Kanaoka, Y., Minamino, N. et al. (1984). Primary structure of Electrophorus electricus sodium channel deduced from cDNA sequence. *Nature* **312**, 121-127.
Papazian, D. M., Shao, X. M., Seoh, S. A., Mock, A. F., Huang, Y. and Wainstock, D. H. (1995). Electrostatic interactions of S4 voltage sensor in Shaker K^+ channel. *Neuron* **14**, 1293-1301.
Peitsch, M. C. (1997). Large scale protein modelling and model repository. *Proc. Int. Conf. Intell. Syst. Mol. Biol.* **5**, 234-236.
Peitsch, M. C., Wells, T. N., Stampf, D. R. and Sussman, J. L. (1995). The Swiss-3DImage collection and PDB-Browser on the World-Wide Web. *Trends Biochem. Sci.* **20**, 82-84.
Perozo, E. (2000). Structure and packing orientation of transmembrane segments in voltage-dependent channels. Lessons from perturbation analysis [comment]. *J. Gen. Physiol.* **115**, 29-32.
Perozo, E., MacKinnon, R., Bezanilla, F. and Stefani, E. (1993). Gating currents from a nonconducting mutant reveal open-closed conformations in Shaker K^+ channels. *Neuron* **11**, 353-358.
Perozo, E., Cortes, D. M. and Cuello, L. G. (1999). Structural rearrangements underlying K^+-channel activation gating. *Science* **285**, 73-78.
Rost, B., Yachdav, G. and Liu, J. (2004). The PredictProtein server. *Nucleic Acids Res.* **32**, W321-W326.
Scholle, A., Koopmann, R., Leicher, T., Ludwig, J., Pongs, O. and Benndorf, K. (2000). Structural elements determining activation kinetics in KV2.1. *Recept. Channels* **7**, 65-75.
Schwede, T., Kopp, J., Guex, N. and Peitsch, M. C. (2003). SWISS-MODEL: An automated protein homology-modeling server. *Nucleic Acids Res.* **31**, 3381-3385.
Seoh, S. A., Sigg, D., Papazian, D. M. and Bezanilla, F. (1996). Voltage-sensing residues in the S2 and S4 segments of the Shaker K^+ channel. *Neuron* **16**, 1159-1167.
Sigg, D. and Bezanilla, F. (1997). Total charge movement per channel. The relation between gating charge displacement and the voltage sensitivity of activation. *J. Gen. Physiol.* **109**, 27-39.
Silverman, W. R., Roux, B. and Papazian, D. M. (2003). Structural basis of two-stage voltage-dependent activation in K^+ channels. *Proc. Natl. Acad. Sci. USA* **100**, 2935-2940.
Starace, D. M. and Bezanilla, F. (2004). A proton pore in a potassium channel voltage sensor reveals a focused electric field. *Nature* **427**, 548-553.
Tiwari-Woodruff, S. K., Schulteis, C. T., Mock, A. F. and Papazian, D. M. (1997). Electrostatic interactions between transmembrane segments mediate folding of Shaker K^+ channel subunits. *Biophys. J.* **72**, 1489-1500.
Tiwari-Woodruff, S. K., Lin, M. A., Schulteis, C. T. and Papazian, D. M. (2000). Voltage-dependent structural interactions in the Shaker K(+) channel. *J. Gen. Physiol.* **115**, 123-138.
Yang, N. and Horn, R. (1995). Evidence for voltage-dependent S4 movement in sodium channels. *Neuron* **15**, 213-218.
Zhang, M., Liu, J. and Tseng, G. N. (2004). Gating charges in the activation and inactivation processes of the HERG channel. *J. Gen. Physiol.* **124**, 703-718.